THE JOURNAL OF BIOLOGICAL CHEMISTRY VOL. 292, NO. 1, pp. 386–396, January 6, 2017

Co-evolution of Two GTPases Enables Efficient Protein Targeting in an RNA-less Chloroplast Signal Recognition Particle Pathway*

Received for publication, August 9, 2016, and in revised form, November 17, 2016 Published, JBC Papers in Press, November 28, 2016, DOI 10.1074/jbc.M116.752931

Sowmya Chandrasekar[‡], Michael J. Sweredoski[§], Chang Ho Sohn[‡], Sonja Hess[§], and Shu-ou Shan[‡1]

From the [‡]Division of Chemistry and Chemical Engineering and the [§]Proteome Exploration Laboratory, Division of Biology and Biological Engineering, Beckman Institute, California Institute of Technology, Pasadena, California 91125

Edited by Thomas Söllner

The signal recognition particle (SRP) is an essential ribonucleoprotein particle that mediates the co-translational targeting of newly synthesized proteins to cellular membranes. The SRP RNA is a universally conserved component of SRP that mediates key interactions between two GTPases in SRP and its receptor, thus enabling rapid delivery of cargo to the target membrane. Notably, this essential RNA is bypassed in the chloroplast (cp) SRP of green plants. Previously, we showed that the cpSRP and cpSRP receptor GTPases (cpSRP54 and cpFtsY, respectively) interact efficiently by themselves without the SRP RNA. Here, we explore the molecular mechanism by which this is accomplished. Fluorescence analyses showed that, in the absence of SRP RNA, the M-domain of cpSRP54 both accelerates and stabilizes complex assembly between cpSRP54 and cpFtsY. Crosslinking coupled with mass spectrometry and mutational analyses identified a new interaction between complementarily charged residues on the cpFtsY G-domain and the vicinity of the cpSRP54 M-domain. These residues are specifically conserved in plastids, and their evolution coincides with the loss of SRP RNA in green plants. These results provide an example of how proteins replace the functions of RNA during evolution.

Proper localization of newly synthesized proteins is essential for survival in all kingdoms of life. In the cytosol, signal recognition particle (SRP)[2] and SRP receptor (SR) are the major molecular machineries that target nascent proteins emerging from the ribosome to the eukaryotic endoplasmic reticulum or the bacterial plasma membrane (1–3). The universally conserved functional core of cytosolic SRP consists of an SRP54 protein tightly bound to an SRP RNA (4, 5). SRP54 is a modular protein with multiple domains. A methionine-rich M-domain binds the SRP RNA and interacts with the signal sequence of the cargo protein. An N-terminal N-domain interacts with the ribosome, and a GTPase G-domain binds and hydrolyzes GTP (6–9). The N- and G-domains pack tightly with one another to form a structural and functional unit termed the NG-domain, which directly interacts with a highly homologous NG-domain in the SR (called FtsY in bacteria). The GTP-dependent interaction between the NG-domains of SRP and SR mediates the delivery of cargo to the proper cellular membrane. Subsequent GTP hydrolysis in the SRP-SR NG-domain complex drives their disassociation, thus recycling SRP and its receptor for additional rounds of targeting (10, 11).

A notable exception to the classic cytosolic SRP is found in chloroplast (12, 13). Chloroplast SRP54 (cpSRP54) participates in two pathways in the chloroplast stroma. One pool mediates the co-translational targeting of thylakoid membrane proteins synthesized by the chloroplast ribosome, such as the polytopic D1 thylakoid membrane protein. Another pool associates with a novel protein subunit cpSRP43 to form the chloroplast SRP (cpSRP), which mediates the post-translational targeting of the light-harvesting chlorophyll a/b-binding proteins to the thylakoid membrane (12, 14–16). Both pathways retain homologues of the SRP and SR GTPases (termed cpSRP54 and cpFtsY, respectively) (17–19). Surprisingly, the otherwise universally conserved SRP RNA is lost in cpSRP during the evolution of green plants from cyanobacteria (20, 21).

Previous observations provide clues as to how cpSRP tolerates the loss of the SRP RNA. Studies in the bacterial SRP pathway showed that the major role of SRP RNA is to regulate the activity of the SRP and FtsY GTPases. Complex assembly between the SRP and FtsY NG-domains is intrinsically very slow and insufficient to sustain protein targeting. The SRP RNA accelerates SRP-FtsY assembly 10^2–10^4-fold when SRP is loaded with ribosomes bearing correct SRP substrates and thus ensures rapid and selective delivery of the correct cargos to the target membrane (22, 23). The SRP RNA also stimulates GTP hydrolysis from the SRP·FtsY complex at the end of the targeting reaction and thus allows efficient recycling of SRP and SR (24, 25). Intriguingly, kinetic studies in the cpSRP system found that the two GTPases in cpSRP54 and cpFtsY can bind and activate each other efficiently in the absence of SRP RNA (26, 27), providing an initial clue for how cpSRP bypasses the requirement for the essential SRP RNA. Subsequent crystallo-

* This work was supported by National Institutes of Health Grant 1R01GM114390 and fellowships from the Gordon and Betty Moore Foundation and American Federation for Aging Research (to S. S.). The authors declare that they have no conflicts of interest with the contents of this article. The content is solely the responsibility of the authors and does not necessarily represent the official views of the National Institutes of Health.

[1] To whom correspondence should be addressed. Tel.: 626-395-3879; Fax: 626-568-9430; E-mail: sshan@caltech.edu.

[2] The abbreviations used are: SRP, signal recognition particle; SR, SRP receptor; cp, chloroplast; IPTG, isopropyl 1-thio-β-D-galactopyranoside; DACM, *N*-(7-dimethylamino-4-methylcoumarin-3-yl)-maleimide; BODIPY-FL, BODIPY-fluorescein-*N*-(2 aminoethyl)-maleimide; SCX, strong cation exchange; acrylodan, 6-acryloyl-2-dimethylaminonaphthalene; GppNHp, guanosine 5′-[β,γ-imido]triphosphate.

graphic analyses showed that cpFtsY is conformationally better organized to interact with cpSRP54 than bacterial FtsY (28–30). This effect, however, contributes only 5–10-fold to the 400-fold faster assembly between cpSRP54 and cpFtsY compared with their bacterial homologues. More recently, cross-complementation analysis showed that the M-domain of SRP54 stimulates GTPase assembly and activation in the chloroplast but not the cytosolic SRP system (27). This strongly suggests that the cpSRP54 M-domain might have replaced the function of the SRP RNA. Nevertheless, the molecular mechanism underlying the stimulatory effect of the M-domain is not understood.

In this work, we address the following questions. How does the cpSRP54 M-domain stimulate the interaction between cpSRP54 and cpFtsY? What molecular interactions mediate its stimulatory effect? How did the cpSRP system evolve to use the M-domain in place of the SRP RNA? Using a combination of fluorescence, cross-linking, and mass spectrometry experiments, we identified a new pair of electrostatic interactions between cpFtsY and the cpSRP54 M-domain. The importance of this interaction is supported by mutagenesis analyses and by phylogenetic conservation of the interacting residues strictly among the plastid but not the cytosolic SRP components. The emergence of this new site coincides with the loss of SRP RNA during the evolution of photosynthetic organisms, providing an example for how proteins could evolve to replace the function of RNA.

Results

M-domain of cpSRP54 Is Essential for Both the Assembly and Stability of the cpSRP54·cpFtsY Complex—Free cpSRP54 and cpFtsY exhibit low basal GTPase rates, but GTP hydrolysis is enhanced 10^3–10^4-fold when the two GTPases form a complex with one another (26). A previous analysis, which monitors this reciprocally activated GTPase reaction between cpSRP54 and cpFtsY, showed that the cpSRP54 M-domain stimulates this GTPase reaction 50-fold (27). To directly test whether the cpSRP54 M-domain promotes complex formation between cpSRP54 and cpFtsY, we used a Föster resonance energy transfer (FRET) assay. The donor (DACM) was labeled at an engineered cysteine at residue 234 of Cys-lite cpSRP54 (in which the solvent-exposed Cys-198 was mutated to a serine (31)). The acceptor (BODIPY-FL) was labeled at an engineered cysteine at residue 321 of Cys-less cpFtsY (31). The cysteine mutations and fluorescence labeling do not affect complex assembly between cpSRP54 and cpFtsY (31). For simplicity, the engineered proteins are referred to as wild-type cpSRP54 and cpFtsY.

Using the FRET assay, we determined the association rate constants (k_{on}) of the cpSRP54·cpFtsY complex for full-length cpSRP54 (with M-domain) and cpSRP54-NG (lacking the M-domain). The results show that full-length cpSRP54 assembles a stable complex with cpFtsY 200-fold faster than cpSRP54-NG, with rate constants of 5×10^5 and 2.8×10^3 M^{-1} s^{-1}, respectively (Fig. 1*A*). This provides direct evidence for and more accurate measurement of the rate advantage provided by the cpSRP54 M-domain during cpSRP54·cpFtsY complex assembly.

To test whether the M-domain also stabilizes the cpSRP54·cpFtsY complex, we performed equilibrium titrations using the FRET assay (Fig. 1*B*). Interestingly, cpSRP54-NG assembles a much weaker complex with cpFtsY than full-length cpSRP54, with an equilibrium constant (K_d) of 12 μM as compared with 0.77 μM for full-length cpSRP54 (Fig. 1*B*). Thus, the cpSRP54 M-domain is also required for formation of a stable cpSRP54·cpFtsY complex. This is slightly different from the 4.5S SRP RNA in the bacterial SRP, which only affects the kinetics, but not the thermodynamic stability, of the corresponding SRP·FtsY complex (22, 25).

Finally, dissociation of the cpSRP54-NG·cpFtsY complex exhibits distinct kinetics from that of the full-length cpSRP54·cpFtsY complex (Fig. 1*C*). The full-length cpSRP54·cpFtsY complex exhibits single exponential kinetics during its disassembly, with a disassociation rate (k_{off}) of 0.02 s^{-1} (Fig. 1*C*, *blue*) (31). In contrast, disassembly of the cpSRP54-NG·cpFtsY

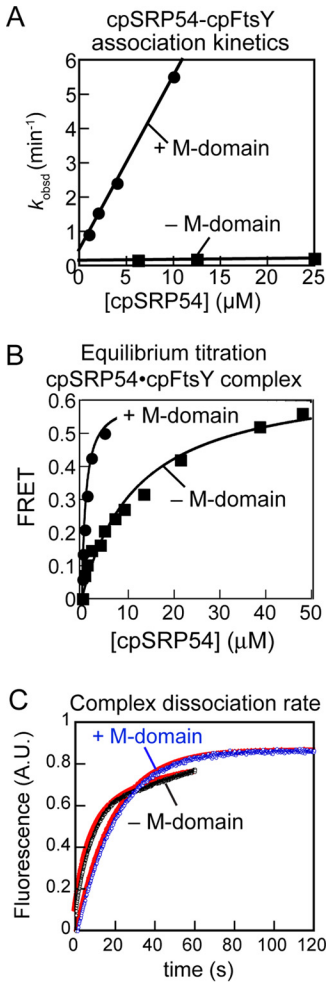

FIGURE 1. **cpSRP54 M-domain accelerates and stabilizes the cpSRP54·cpFtsY complex.** *A*, association rate constant (k_{on}) for complex formation of cpFtsY with cpSRP54 (●) and cpSRP54-NG (■), measured using the FRET assay as described under "Experimental Procedures." Linear fits of the data to Equation 2 gave rate constants of 5×10^5 and 2.8×10^3 M^{-1} s^{-1} in the presence and absence of the M-domain, respectively. *B*, equilibrium titrations of the cpSRP54·cpFtsY (●) or cpSRP54-NG·cpFtsY (■) complex in the presence of GTP using FRET. The data with cpSRP54 and cpSRP54-NG were fit to Equations 4 and 5, respectively, which gave K_d values of 0.77 and 12 μM in the presence and absence of M-domain, respectively. *C*, representative time courses for disassociation of the cpSRP54·cpFtsY (*blue*) and cpSRP54NG·cpFtsY complexes (*black*), measured using pulse-chase experiments as described under "Experimental Procedures." The data with cpSRP54-NG were fit to Equation 3, which gave rate constants of 0.140 and 0.0123 s^{-1} for the first and second phases, respectively. The data with cpSRP54 were fit to a single exponential function, which gave a k_{off} value of 0.02 s^{-1}.

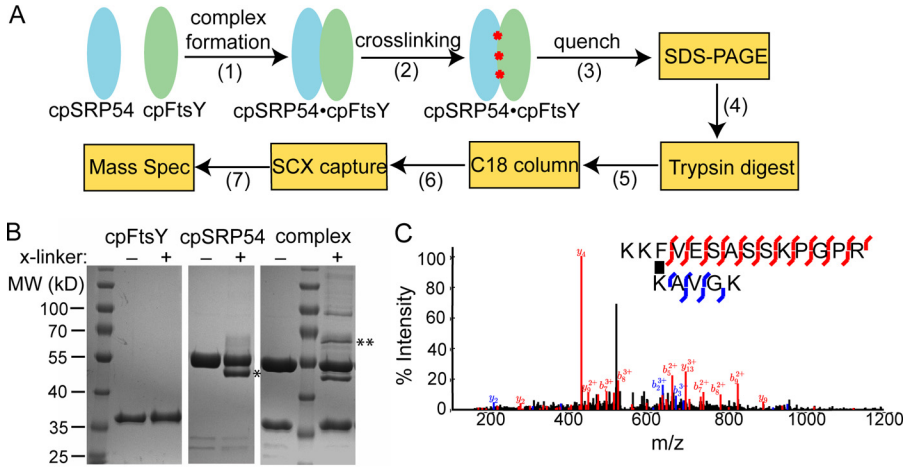

FIGURE 2. **Cross-linking and mass spectrometry to identify the interaction site of the cpSRP54 M-domain with cpFtsY.** *A,* schematic for the workflow of the cross-linking/MS experiment. Details are described under "Experimental Procedures." *B,* representative SDS-PAGE analysis of the cross-linking reaction with cpFtsY alone (*left gel*), cpSRP54 alone (*middle gel*), and the cpSRP54·cpFtsY complex formed in GTP (*right gel*). − and + denote the absence and presence of cross-linker, respectively. ** denotes the cross-linked cpSRP54·cpFtsY complex used for MS analysis. * denotes an intra-molecular cross-link of cpSRP54 (*middle gel*). *C,* MS/MS spectrum of quadruply charged inter-protein cross-linked peptide ion (shown in *black*), comprising KKFVESASSKPGPR from cpSRP54 and KAVGK from cpFtsY. Observed b and y fragment ions are shown in *red* and *blue* for cpSRP54 and cpFtsY, respectively.

complex exhibits biphasic kinetics with an initial fast phase occurring at 0.14 s^{-1} followed by a second phase that occurs at 0.012 s^{-1} (Fig. 1*C*, *black*). The weighted average of the two phases is ~0.0380 s^{-1}, consistent with predictions from the k_{on} and K_d values measured above for this complex. This suggests that the bi-phasic dissociation kinetics arises from conformational heterogeneity in the cpSRP54-NG·cpFtsY complex. The alternative model that the biphasic kinetics arose from a sequential mechanism of dissociation could be ruled out, as such a model would predict an overall dissociation rate constant of <0.012 s^{-1} (the overall rate constant of a sequential reaction cannot be faster than the rate constant of any individual steps in the reaction sequence). Thus, the cpSRP54 M-domain is also important for the cpSRP54·cpFtsY complex to assume a homogeneous conformation. This is consistent with the observation that the presence of the M-domain also enhances GTPase activation in the cpSRP54·cpFtsY complex (27).

M-domain of cpSRP54 Directly Interacts with cpFtsY—The cpSRP54 M-domain could exert its stimulatory effect by interacting with and pre-organizing the cpSRP54-NG-domain or by directly interacting with cpFtsY. To distinguish between these models and pinpoint the molecular contacts used by the M-domain, we used cross-linking combined with mass spectrometry (MS) (Fig. 2*A*). In the absence of a crystal structure of the complete cpSRP54·cpFtsY complex, this approach is highly valuable and has been successfully used to map the interaction surfaces between the bacterial SRP54 and FtsY homologues (38).

We used a clickable cross-linker, NHS-activated 2,2′-(hex-5-ynylazanediyl) diacetic acid, which reacts with lysine side chains at pH 7.0 (32). We cross-linked the cpSRP54·cpFtsY complex formed in the presence of GTP. SDS-PAGE analysis confirmed that a higher molecular weight cross-linked species is specifically formed in the complex but not in free cpSRP54 or cpFtsY (Fig. 2*B*, **). The cross-linked band was excised, trypsin-digested, purified, and analyzed following the schematics depicted in Fig. 2*A*.

MS analysis of the sample identified several candidate intra- and inter-molecular cross-links (Table 1). This is not surprising given that both cpFtsY and cpSRP54 have a large number of lysine residues on their surfaces, and their NG-domains directly interact with one another. In addition, cpSRP54 tends to form intra-molecular cross-links (Fig. 2*B*, *). As our goal was to elucidate the role of the cpSRP54 M-domain in complex assembly, we focused on cross-links between the M-domain and cpFtsY. Among the top scoring cross-linked peptides, a cross-link was reproducibly observed between ^{236}KAGVK from cpFtsY and cpSRP54 M-domain. Fig. 2*C* shows a representative MS/MS spectrum for the cross-linked peptide. The b and y fragment ions cover 88% of the sequence of the cross-linked peptides. The spectra received a score of 24.5 from Protein Prospector, and the precursor mass error was 1.9 ppm. Cross-links to cpFtsY Lys-236 were highly reproducible over multiple trials, although with different lysines in the cpSRP54 M-domain (Table 1). Thus, although the interaction site on the cpSRP54 M-domain could not be identified through cross-linking, these data identified Lys-236 in the G-domain of cpFtsY as a strong candidate for interaction with the M-domain.

The following observations further support this hypothesis. First, Lys-236 and several lysine residues in its vicinity are highly conserved in plastid cpFtsY but not in their cytosolic homologues (Fig. 3, *A* and *B*). In addition, these lysines are adjacent to Ala-233 (Fig. 3*A*, *brown*); this residue has diverged in plastid cpFtsY but corresponds to the highly conserved Lys-399 in *E. coli* FtsY (Fig. 3*B*), which directly interacts with the SRP RNA to accelerate SRP·FtsY complex assembly in the bacterial SRP pathway (39, 40). Thus, the cross-linking experiments provided a good starting point for probing the putative interaction site for the cpSRP54 M-domain on cpFtsY.

Mutations in the Basic Residues of cpFtsY Compromise Interaction between cpSRP54 and cpFtsY—Sequence analysis of SRP receptors identified two patches of basic residues that are uniquely conserved among plastid cpFtsYs but not in their

TABLE 1
List of intermolecular cross-linked peptides between cpSRP54 and cpFtsY observed in LC-MS/MS analysis

m/z	*z*	ppm	Score	Cross-linked peptide	Protein
549.819	4	1.9	24.5	K(1693.9152)AVGK KK(678.4065)FVESASSKPGPR	cpFtsY cpSRP54
549.8166	4	−2.4	15.7	K(1693.9152)AVGK K(678.4065)KFVESASSKPGPR	cpFtsY cpSRP54
432.239	4	−0.85	14.9	VFSGFSK(697.3833)TR VK(1204.6241)M(oxidation)K	cpFtsY cpSRP54
479.2574	4	−0.095	8.8	K(1437.7252)NSK FVESASSK(652.3544)PGPR	cpFtsY cpSRP54
382.4894	4	1.3	7	LIK(697.3833)EKAK VK(1005.6223)M(oxidation)K	cpFtsY cpSRP54
940.5127	3	1.6	6.2	EK(1033.5808)AKSDVEKVFSGFSK EVSGK(1962.0098)PIK	cpFtsY cpSRP54
509.6503	3	1.6	5.8	LIKEK(697.3833)AK VK(1005.6223)M(oxidation)K	cpFtsY cpSRP54
1458.4985	3	3.4	4.9	KPAVIMIVGVNGGGK(2346.2981)TTSLGK SGPTVILLAGLQGVGK(2203.2399)TTVC(carbamidomethyl)AK	cpFtsY cpSRP54

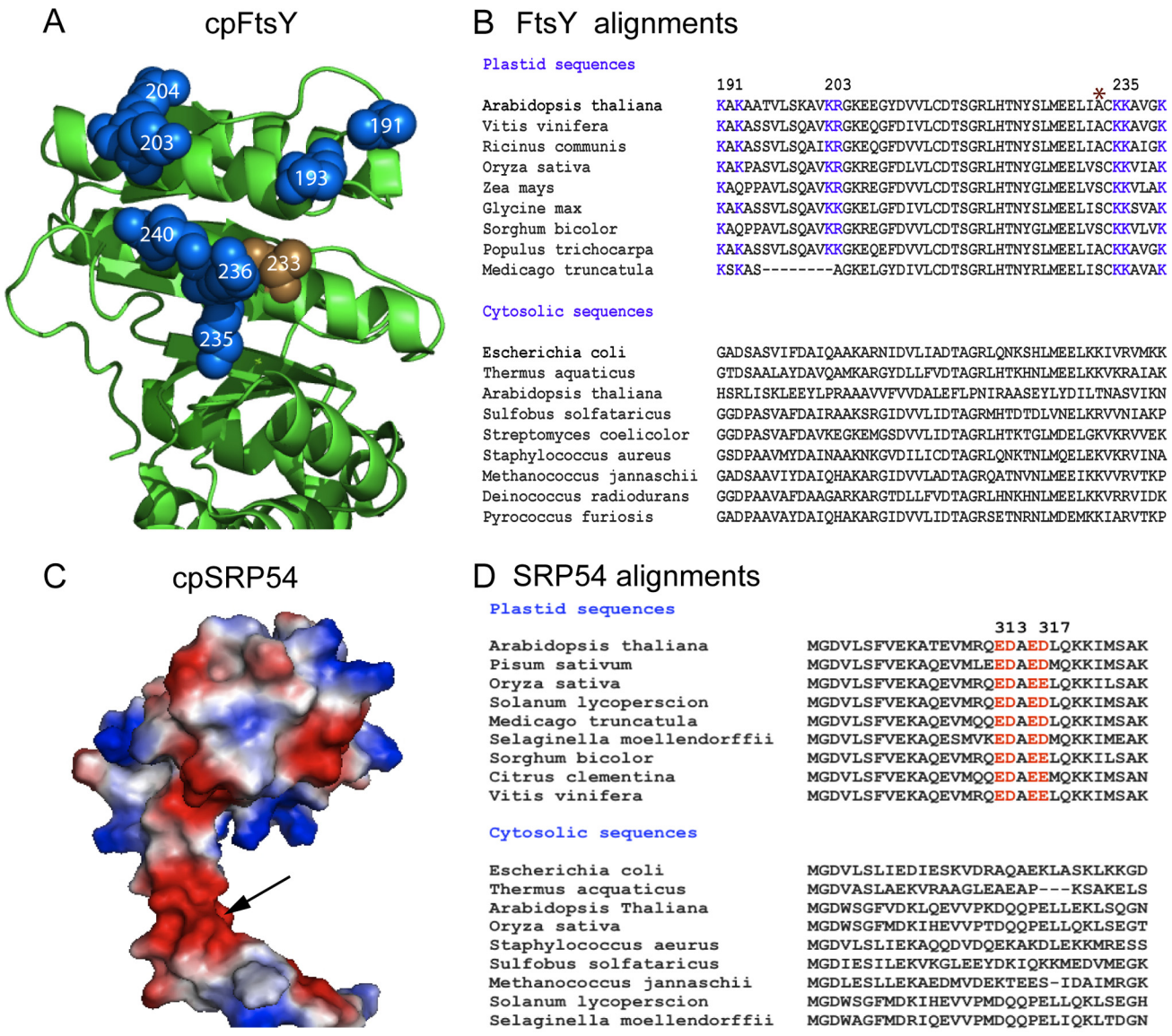

FIGURE 3. **Sequence alignments reveal conserved and complementarily charged regions in cpSRP54 and cpFtsY.** *A,* crystal structure of cpFtsY (*green*, Protein Data Bank code 2OG2), highlighting the clusters of positively charged residues identified from cross-linking data (*blue*). Ala-233, which corresponds to Lys-399 in *E. coli* FtsY, is indicated in *brown*. *B,* sequence alignments of plastid cpFtsY and cytosolic SR homologues. The conserved basic residues are shown in *blue*. * highlights the residue corresponding to Lys-399 in *E. coli* FtsY, which was mutated to Ala or Ser in cpFtsYs. *C,* electrostatic surface map of a homology model of the cpSRP54 M-domain, showing basic residues in *blue* and acidic residues in *red.* The *arrow* indicates the acidic residues highlighted in part (*D*). *D,* sequence alignment of the N-terminal residues in the M-domains of chloroplast and cytosolic SRP54 homologues. The conserved acidic residues unique to plastid cpSRP54 are shown in *red*.

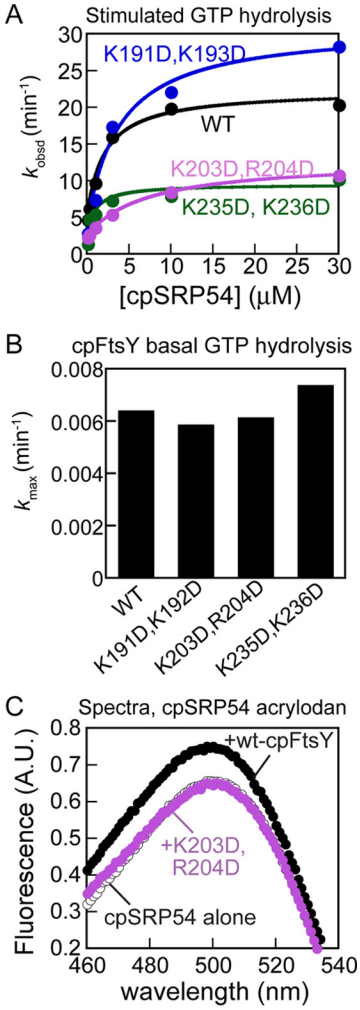

FIGURE 4. **Mutational analyses of basic residues in cpFtsY.** *A,* representative stimulated GTPase reactions of cpSRP54 with wild-type cpFtsY (*black*) and mutants cpFtsY(K191D/K193D) (*blue*), cpFtsY(K203D/R204D) (*purple*), and cpFtsY(K234D/K235D) (*green*), measured and analyzed as described under "Experimental Procedures." Lines are fits of the data to Equation 6. *B,* basal GTP hydrolysis rate constants for wild-type and mutant cpFtsY, determined as described under "Experimental Procedures." *C,* fluorescence emission spectra for acrylodan-labeled cpSRP54 by itself (○) and in the presence of wild-type cpFtsY (●) or mutant cpFtsY(K203D/R204D) (*purple*).

cytosolic homologues. This includes Lys-235 and Lys-236 identified by the cross-linking and MS analyses, as well as Lys-203, Arg-204, Lys-191, and Lys-193 (Fig. 3, *A* and *B*, *blue*). All these residues are away from the conserved interaction surface between the NG-domains of SRP54 and FtsY from bacterial, archaeal, and chloroplast SRP systems (28, 29).

To test whether these residues are involved in the cpSRP54-cpFtsY interaction, we constructed the following three sets of charge reversal mutants (Fig. 4*A*): K203D/R204D, K235D/K236D, and K191D/K193D. Interaction between cpSRP54 and cpFtsY was first tested using the GTPase assay that monitors their reciprocally stimulated GTPase reaction. This assay, although less sensitive than fluorescence-based assays, can report on the effects of the mutations on both cpSRP54·FtsY complex assembly and their GTPase activation (22, 26, 31, 41). For wild-type cpSRP54 and cpFtsY, the value of k_{cat}/K_m is rate-limited by and hence reports on the rate constant for assembly of a stable cpSRP54·cpFtsY complex; the value of k_{cat} reports on the overall rate constant of activated GTP hydrolysis from the complex (22, 26). The results showed that mutant cpFtsY(K191D/K193D) had no effect (Fig. 4*A*, *blue*). In contrast, both mutants cpFtsY(K203D/R204D) and cpFtsY(K235D/K236D) were compromised in GTPase assembly and/or activation (Fig. 4*A*, *purple* and *green*). The k_{cat}/K_m and k_{cat} values for cpFtsY(K203D/R204D) were reduced by 5- and 2.5-fold, respectively, whereas the k_{cat} value for cpFtsY(K235D/K236D) was reduced ~3.5-fold. The basal GTP hydrolysis rates of free cpFtsY were unaffected by these mutations (Fig. 4*B*), strongly suggesting that the mutational defects did not arise from misfolding of the mutant proteins.

To independently test the effect of these mutations on cpSRP54·cpFtsY complex assembly, we used a fluorescence assay based on cpSRP54 labeled with an environmentally sensitive dye, acrylodan, at Cys-234 at the NG-domain interface. This probe senses a conformational change at the interface between N- and G-domains and exhibits enhanced fluorescence upon formation of a stable cpSRP54·cpFtsY complex (Fig. 4*C*, *open versus closed black circles* (23, 31)). In contrast, with mutant cpFtsY(K203D/R204D), no change in the fluorescence of acrylodan-labeled cpSRP54(Cys-234) was observed (Fig. 4*C*, *purple*). This directly shows that this patch of basic residues in cpFtsY participates in cpSRP54·cpFtsY complex assembly, despite being >35 Å away from the interaction interface between their NG-domains.

A Complementarily Charged Region in cpSRP54 M-domain Interacts with cpFtsY—The above observations suggest that the basic cluster in the G-domain of cpFtsY could provide an interaction site for the cpSRP54 M-domain, potentially by mediating an electrostatic interaction. This hypothesis is supported by the following observations. First, GTPase assays showed that cpSRP54-cpFtsY assembly, as monitored by the value of k_{cat}/K_m, is 14-fold slower at higher salt concentrations (Fig. 5*A*), consistent with an electrostatically driven interaction during the assembly process. In addition, analysis of the electrostatic surface potential of the cpSRP54 M-domain revealed a highly negatively charged region at the N terminus of the M-domain (Fig. 3, *C* and *D*, Glu-313, Asp-314, Glu-316, and Asp-317). Finally, sequence comparisons showed that this set of acidic residues is highly conserved among plastid cpSRP54s but was divergent in cytosolic SRP54 homologues (Fig. 3*D*).

To test whether this patch of acidic residues at the cpSRP54 M-domain is important for the cpSRP54-cpFtsY interaction, we generated two sets of charge reversal mutant, cpSRP54 (E313K/D314K) and cpSRP54(E316K/D317K). In addition, we made a quadruple mutant in which all four acidic residues were replaced by lysines. In stimulated GTPase reactions, both mutants E313K/D314K and E316K/D317K exhibited 2-fold reductions in the values of k_{cat}/K_m, indicating defects in cpSRP54-cpFtsY assembly (Fig. 5*B*). In addition, mutant cpSRP54 (E316K/D317K) also reduced the value of k_{cat} 2-fold, indicating that GTPase activation between cpSRP54 and cpFtsY is slightly compromised (Fig. 5*B*).

Much stronger defects were observed with the quadruple mutant; the k_{cat}/K_m value was reduced ~17-fold, and the k_{cat} value was reduced 12-fold (Fig. 5*B*, *red*). The basal GTP hydrolysis rates for all the charge-reversed cpSRP54 mutants were

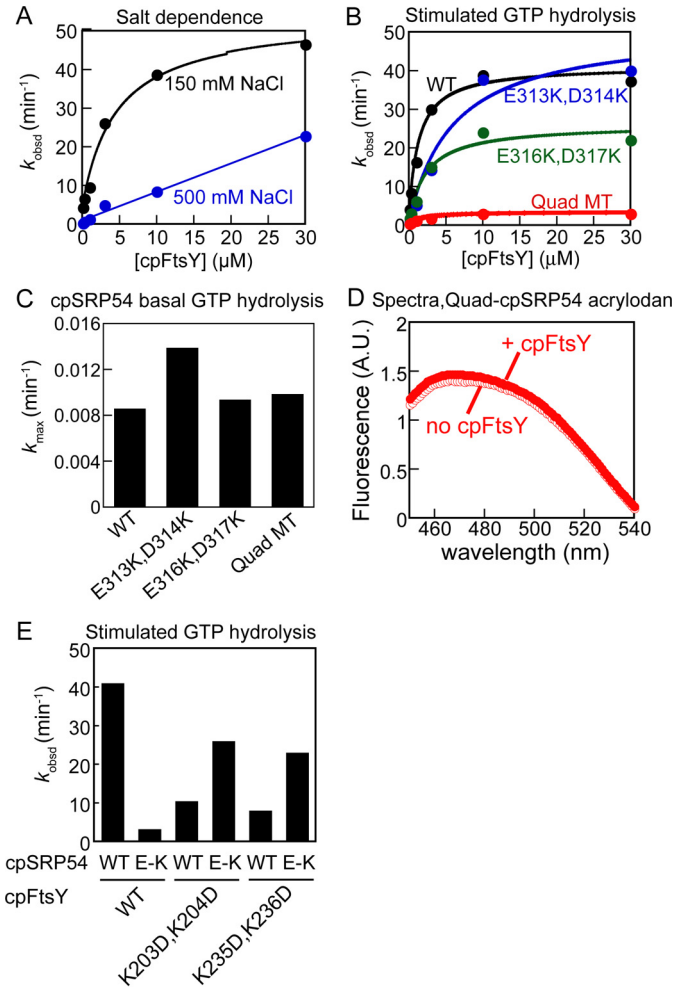

FIGURE 5. **Mutational analyses of acidic residues in the cpSRP54 M-domain.** *A,* representative stimulated GTPase reactions between cpSRP54 and cpFtsY, determined at 150 mM (*black*) and 500 mM NaCl (*blue*). *Lines* are fits of the data to Equation 6. *B,* representative stimulated GTPase reaction of cpFtsY with wild-type cpSRP54 (*black*) and mutants cpSRP54(E313K/D314K) (*blue*), cpSRP54(E316K/D317K) (*green*), or cpSRP54 quadruple mutant (*red*). *Lines* are fits of the data to Equation 6. *C,* basal GTP hydrolysis rate constants of wild-type and mutant cpSRP54, determined as described under "Experimental Procedures." *D,* fluorescence emission spectra of acrylodan-labeled at Cys-234 in the cpSRP54 quadruple mutant in the absence (*open circles*) and presence (*closed circles*) of wild-type cpFtsY. *E,* summary of the GTP hydrolysis rate constants (k_{cat}) for the stimulated GTPase reaction between wild-type and charge-reversed mutants of cpSRP54 and cpFtsY. *E-K* denotes the cpSRP54 quadruple mutant.

comparable with wild-type cpSRP54 (Fig. 5*C*), strongly suggesting that the observed defects did not arise from misfolding of the mutant protein. To directly probe the role of this acidic site in complex assembly between cpSRP54 and cpFtsY, we used acrylodan-labeled cpSRP54(Cys-234) containing the quadruple mutation. No change in fluorescence emission spectra was observed upon addition of cpFtsY to the cpSRP54 quad mutant (Fig. 5*D*). Thus, the acidic residues adjacent to the M-domain are important for cpSRP54·cpFtsY complex assembly and GTPase activation.

Finally, if the basic site identified in cpFtsY and the acidic site at the cpSRP54 M-domain directly interacts with one another electrostatically, then combining the two charge-reversed mutants would rescue GTPase assembly and activation. This was indeed observed. In the reaction of the cpSRP54 quad mutant with cpFtsY K203D/R204D or K235D/K236D, efficient GTPase activation was restored (Fig. 5*E*). Collectively, these results provide strong evidence that the M-domain of cpSRP54 has evolved a distinct site to interact with cpFtsY electrostatically, thus replacing the SRP RNA to stimulate the assembly and activation between the SRP54 and FtsY GTPases.

Phylogenetic Analysis of Interaction Motifs in the cpSRP Pathway—To better understand how this new set of interactions evolved in the cpSRP pathway, we performed a phylogenetic analysis. Previously, Schunemann and co-workers (20, 21) carried out a thorough analysis that identified SRP RNA genes and predicted their secondary structure across all lineages of photosynthetic organisms, ranging from red and blue algae to land green plants. This analysis showed that the SRP RNA exists in some branches of blue and red algae and is lost during the evolution to higher green plants. Based on this information and the available evolutionary lineage and distances of photosynthetic organisms, we searched for the appearance of the charged residues identified here in cpSRP54 and cpFtsY sequences from 24 annotated plastid genomes. The sequence of the SRP RNA tetraloop, the presence of FtsY Lys-399 that interacts with this loop, and the presence of the SM-G*X*G motif in the SRP54 M-domain critical for RNA binding were used as additional information to decipher when the cpSRP54 M-domain replaced the SRP RNA (42).

As expected, the emergence of the new basic site on cpFtsY to the acidic site on cpSRP54 strongly correlates with one another and with the absence of SRP RNA or a functional RNA tetraloop (*e.g. Physcomitrella patens*) in ferns, liverworts, and higher green plants (Table 2 and Fig. 6). The appearance of this new interaction site also strongly correlates with mutation of the conserved RNA-binding motif in the cpSRP54 M-domain (Table 2). The nearest evolutionary neighbor to land green plants, the soil alga *Chlorokybus atmophyticus*, still preserves a functional SRP RNA and its interaction sites on cpSRP54 and cpFtsY, whereas the new cpSRP54 M-cpFtsY interaction sites are incomplete. This strongly suggests that the evolution to replace the SRP RNA begins with the ancestor for the embryophyta or the land plants branch of green plants.

Intriguingly, the SRP RNA is absent in several other branches of photosynthetic organisms. In the chloroplast of green algae, although many species preserved a functional SRP RNA, *Chlamydomonas reinhardtii* and *Volvox carteri* have lost the SRP RNA and the RNA interaction sites on cpFtsY and cpSRP54 (Table 2 and Fig. 6) (20, 43), and the new interaction sites between the cpFtsY and cpSRP54 M-domain were partially evolved in these species (Table 2). Whether this interaction, or a distinct molecular mechanism, is used by the cpSRP in these species to replace the SRP RNA is unclear. Similar phenomena were observed in lower red and blue algae that are distantly related to land green plants (Table 2 and Fig. 6). These observations strongly suggest that the loss of SRP RNA appears to have occurred independently on multiple occasions during evolution.

TABLE 2

Summary of the components and sequence elements in cpSRP systems from diverse photosynthetic organisms

Species[a]	SRP RNA present?	RNA loop size	FtsY K399	RNA binding site[b]	cpSRP54 acidic cluster	cpFtsY basic cluster
Arabidopsis thaliana	×		×	VM-DSG	ED-ED	KR-KK-K
Vitis vinifera	×		×	AM-DSG	ED-EE	KR-KK-K
Oryza sativa	×		×	VS-ESG	ED-EE	KR-KK-K
Sorghum bicolor	×		×	VM-DSG	ED-EE	KR-KK-K
Selaginella moellendorfii	×		×	AM-ESG	ED-EE	KR-KK-K
Physcomitrella patens	✓	10	×	SM-GSG	ED-EL	RR-KK-K
Chlorokybus atmosphyticus	✓	4(UAAA)	✓	SM-GSG	EQ-KK	QQ-KR-K
Chlamydomonas reinhardtii	×		×	AM-DSG	ED-QK	CK-KA-N
volvox carterii	×		×	AM-DSG	ED-KA	CK-KS-T
Micromonas RCC299	✓	4(GAAA)	×	SM-GAG	EE-EQ	DE-KK-K
Micromonas pusilla	✓	4(GAGA)	×	SM-GSG	EQ-NL	DE-KK-K
Ostreococcus tauri	✓	4(GAAA)	×	SM-GSG	AE-EK	DE-RK-K
Ostreococcus lucimanrius	✓	4(GAAA)	×	SM-GSG	EE-EK	DE-RK-K
Chlorella variabilis	✓	4(GAAA)	✓	SM-GSG	EE-AE	DA-KR-K
Coccomyxa subellisodidea	✓	4(GUAA)	✓	SM-GAG	ED-AE	EQ-KR-K
Bigelowella natans	✓	4(AAAA)	✓	SM-GSG	EA-KT	EA-YK-K
Cyanidioschyzon merolae	✓	4(GGAA)	✓	SM-GSG	KE-QE	KR-RR-R
Phaeodactylum tricornutum	✓	4(GTAA)	✓	SM-GSG	AD-LK	DK-KK-K
Thalassiosira pseudonana	✓	4(GTAA)	✓	SM-GSG	AD-AK	DK-KR-K
Aureococcus anaphagefferens	✓	4(GAAA)	✓	SM-GSG	AE-KA	DV-RR-K
Ectocarpus siliculous	×		×	VM-DAG	EE-AK	EK-KK-D
Fragilaropsis cylindrus	×		×	SM-FSD	EE-RR	DK-KE-E
Emilania huxleyi	×		×	QM-AAG	DE-EA	AK-SD-P
Cyanophora paradoxa	×		×	AM-GSG	DE-EQ	EK-KQ-M

[a] Species lineages are denoted by color, with *green* denoting green algae and higher green plants, *blue* denoting blue algae, and *red* denoting red algae.
[b] The SRP RNA-binding site in the cpSRP54 M-domain is an obligatory SM-GXG motif.

Discussion

Throughout evolution, proteins have gradually replaced many functions of RNA. Although many cellular machineries, such as the ribosome, the spliceosome, and RNase P, still preserve the RNA component to carry out their core functions, in specialized cellular organelles proteins appear to continue to replace RNAs even in the highly conserved ribosome. For example, recent cryoEM structures of mammalian mitochondrial ribosome showed that they contain several novel proteins unique to the mitochondria that have replaced specific rRNAs (44, 45). Likewise, the RNA in the classic SRP has been replaced by a protein domain in cpSRP (20, 42, 43). Comparison of the classic and chloroplast SRP provides a simple and attractive system to understand how proteins evolve to replace the functions of RNA.

The results here provide direct evidence that the cpSRP54 M-domain replaces the SRP RNA. The SRP RNA is essential for protein targeting by SRP by accelerating the assembly of the SRP·SR GTPase complex and their reciprocal GTPase activation. In the chloroplast of higher green plants, this otherwise universally conserved RNA is not found. Instead, the cpSRP54 M-domain provides both functions of the SRP RNA; it accelerates complex assembly between cpSRP54 and cpFtsY by 100–200-fold and stimulates GTP hydrolysis in the complex by 10-fold (27). In addition, the results here show that the cpSRP54 M-domain also stabilizes the cpSRP54·cpFtsY complex, in contrast to the strictly catalytic role of the bacterial SRP RNA (22, 25).

This work shows that the cpSRP54 M-domain acquired these new functions by evolving a new set of electrostatic interactions with the cpFtsY G-domain. In bacterial SRP, the conserved tetraloop of 4.5S SRP RNA interacts with FtsY Lys-399 (Fig. 7*B*) (39, 46). Lys-399 is highly conserved in cytosolic SRP receptors

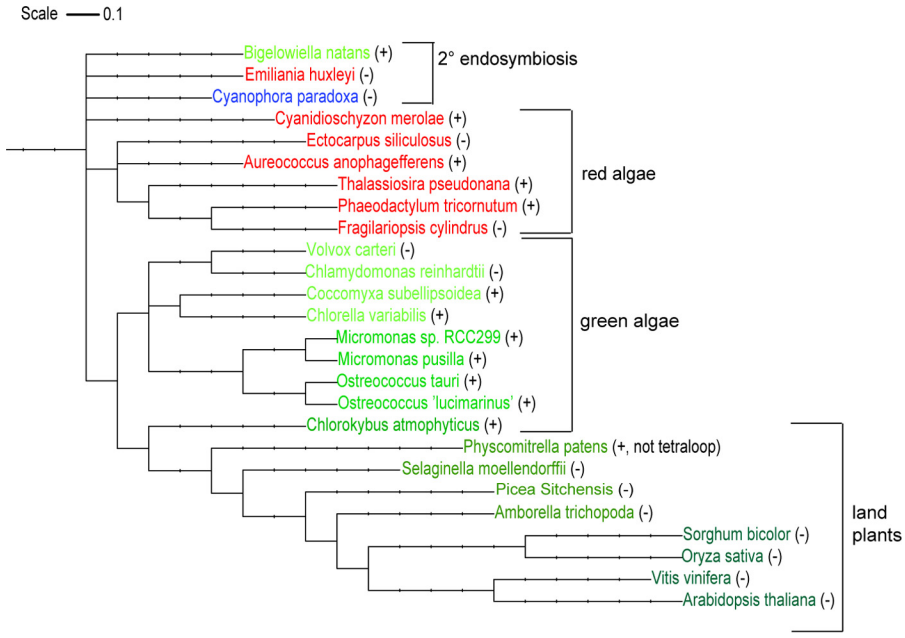

FIGURE 6. **Phylogenetic tree showing the evolution of different chloroplast-containing lineages.** *Blue* denotes blue algae, *red* denotes red algae, and *green* denotes green algae and higher green plants. + and − denote the presence and absence of SRP RNA, respectively. The *scale bar* length represents 0.1 nucleotide substitution/site.

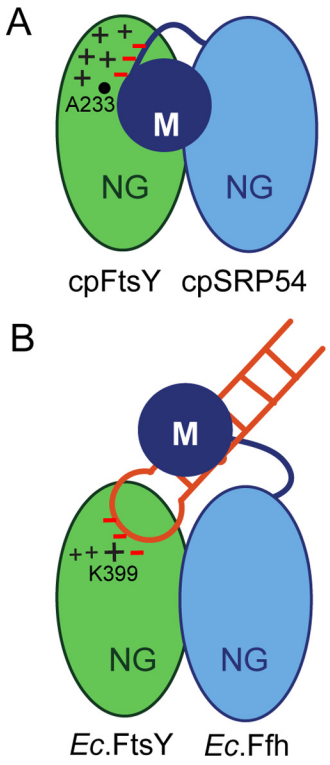

FIGURE 7. **cpSRP pathway bypasses the requirement for SRP RNA by evolving its M-domain to directly modulate complex formation with cpFtsY.** In cpSRP (*A*), the acidic residues N-terminal to the cpSRP54 M-domain directly contact the basic residues in cpFtsY, providing an additional interaction to stabilize the cpSRP54·cpFtsY dimer and the transition state leading to its formation. In the bacterial SRP (*B*), the SRP RNA uses the GNRA tetraloop to interact with the conserved Lys-399 in bacterial FtsY, providing a transient tethering interaction to facilitate efficient complex assembly.

but is mutated to neutral residues in cpSRPs (39). Here, we found that a new collection of basic residues has evolved in cpFtsYs in the vicinity of Lys-399. Correspondingly, a new cluster of acidic residues has evolved at the N terminus of the cpSRP54 M-domain. Analysis of charge-reversal mutants strongly suggests an interaction between these two complementarily charged sites.

The SRP RNA accelerates SRP·FtsY complex formation by providing a transient tethering interaction between the two GTPases during their assembly. The finding that the cpSRP54 M-domain directly interacts with a site in cpFtsY away from the putative NG-domain docking interface (38, 47) strongly suggests that the M-domain exerts its stimulatory effects by providing an analogous tether, rather than pre-organizing the cpSRP54 NG-domain. Structurally, the finding of this interaction also suggests that the M-domain could be adjacent to the NG-domain dimer interface in the active targeting complex (Fig. 7*A*), consistent with the ability of the M-domain to also stimulate GTP hydrolysis in the complex.

Phylogenetic analysis of the interaction motifs in cpSRP54, cpFtsY, and SRP RNA further supports this new interaction site between cpFtsY and the cpSRP54 M-domain. This analysis also showed the loss of plastid SRP RNA has occurred multiple times in several branches of photosynthetic organisms, ranging from blue and red algae to higher green plants, after divergence from their common ancestor. These observations suggest that the evolutionary barrier to the loss of SRP RNA and its replacement with a protein is relatively low. In support of this notion, a number of basic residues are already present in bacterial FtsY in the vicinity of Lys-399, although these residues play a minor role in the function of bacterial SRP (39). It could be envisioned that the preservation of these charges and the appearance of additional basic residues nearby could allow cpFtsY to evolve a new site to interact with cpSRP54, adjacent to its RNA-interacting site in cytosolic FtsY homologues.

Experimental Procedures

Protein Expression and Purification—cpSRP54 and cpFtsY from *Arabidopsis thaliana* were overexpressed and purified as described previously (31). Briefly, cpSRP54 in pET41a (Novagen) was overexpressed in *Escherichia coli* Rosetta cells (Invitrogen) at 37 °C using 0.5 mM IPTG (Biopioneer Inc.) and was purified through SP-Sepharose FF resin (GE Healthcare) followed by cation exchange chromatography over Mono S (GE Healthcare). His_6-tagged cpFtsY in pET32a was overexpressed in BL21-DE3 Star cells (Invitrogen) at 37 °C using 0.5 mM IPTG and purified through Talon resin (Clontech) followed by anion exchange chromatography over a Mono Q column (GE Healthcare).

cpSRP54 and cpFtsY mutants were constructed using the QuikChange protocol (Agilent Technologies) and expressed and purified as for the wild-type proteins with the following exception. cpSRP54-NG was His_6-tagged and purified with Ni-NTA-agarose resin (Qiagen) followed by cation exchange chromatography over a Mono S column.

Fluorescence Labeling and Measurement—Single cysteine mutants were labeled and purified as described previously (31). For FRET experiments, cpSRP54 was labeled with DACM (Molecular Probes) as the donor fluorophore. cpFtsY was labeled with BODIPY-FL (Molecular Probes) as the acceptor fluorophore. For experiments based on environmentally sensitive fluorescence changes, cpSRP54 was labeled with acrylodan (Molecular Probes) (31). Labeling efficiency was typically >80% for all dyes, with <10% background (assessed from parallel reaction with Cys-lite control (31)).

All measurements were performed at 25 °C in assay buffer (50 mM KHEPES (pH 7.5), 150 mM KOAc, 2 mM $Mg(OAc)_2$, 0.01% Nikkol, 10% glycerol). Fluorescence spectra and equilibrium titrations were obtained on a FluoroLog 3-22 spectrofluorometer (Jobin Yvon). Kinetic measurements were performed using a KinTek stopped-flow apparatus. To form the GTP-bound cpSRP54·cpFtsY or cpSRP54-NG·cpFtsY complex, 2 mM GTP (Sigma) was used; GDP released during the course of the reaction was minimal, as explained previously (31). FRET measurements used an excitation wavelength of 380 nm and an emission wavelength of 450 nm. Fluorescence measurements based on acrylodan-labeled cpSRP54 used an excitation wavelength of 370 nm and an emission wavelength of 450 nm. The FRET efficiency (E) was calculated using Equation 1,

$$E = 1 - F_{DA}/F_D \qquad \text{(Eq. 1)}$$

in which F_{DA} and F_D are the fluorescence intensities of donor in the presence and absence of acceptor, respectively.

Association rate constants (k_{on}) for formation of the cpSRP54·cpFtsY complex were measured using 2 μM DACM-labeled cpSRP54 or cpSRP54-NG and indicated concentrations of BODIPY-labeled cpFtsY. The cpFtsY concentration dependence of observed association rate constants (k_{obsd}) was fit to Equation 2,

$$k_{obsd} = k_{on}[\text{cpFtsY}] + k_{off,\ app} \quad \text{(Eq. 2)}$$

in which k_{on} is the association rate constant, and $k_{off,\ app}$ is the apparent rate constant for complex disassembly, contributed by both the dissociation of the ^{GTP}·cpSRP54·cpFtsY·^{GTP} complex and GTP hydrolysis in this complex followed by rapid dissociation of the ^{GDP}·cpSRP54·cpFtsY·^{GDP} complex.

The disassociation rate constant (k_{off}) for the GTP-bound cpSRP54·cpFtsY complex was determined by a pulse-chase experiment. The complex was pre-formed using DACM-labeled cpSRP54 or cpSRP54-NG (2 μM), BODIPY-labeled cpFtsY (30 μM), and 2 mM GTP for 10–20 min and chased with 400 mM EDTA. The time course of fluorescence change (F_{obsd}) during the chase was fit to Equation 3,

$$F_{obsd} = F_e - \Delta F_1 e^{-k_1 t} - \Delta F_2 e^{-k_2 t} \quad \text{(Eq. 3)}$$

in which ΔF_1 and ΔF_2 are the fluorescence changes of the first and second kinetic phases, respectively; k_1 and k_2 are the rate constants for the first and second phases; respectively, and F_e is the fluorescence end point when the reaction reaches equilibrium.

Equilibrium titrations based on FRET were performed using 0.5 μM DACM-labeled wild-type or mutant cpSRP54 and the indicated concentrations of BODIPY-labeled cpFtsY. FRET efficiencies were calculated using Equation 1. With wild-type cpSRP54, the cpFtsY concentration dependence of observed FRET values (E_{obsd}) were fit to Equation 4,

$$E_{obsd} = E_1 \times \frac{([Y] + [54] + K_d) - \sqrt{([54] + [Y] + K_d)^2 - 4[Y][54]}}{2[54]} \quad \text{(Eq. 4)}$$

in which Y is cpFtsY; 54 is cpSRP54; E_1 is the FRET value with saturating cpFtsY, and K_d is the equilibrium dissociation constant of the complex. With cpSRP54-NG, observed FRET values were fit to Equation 5,

$$E_{obsd} = E_1 \times \frac{[\text{cpSRP54}]}{K_d + [\text{cpSRP54}]} \quad \text{(Eq. 5)}$$

in which E_1 and K_d are defined as for Equation 4.

GTPase Assays—GTPase assays were performed at 25 °C in assay buffer as described previously (22, 26). Briefly, reciprocally stimulated GTPase reactions between cpSRP54 and cpFtsY were measured under multiple turnover conditions with 100 nM cpSRP54, varying concentrations of cpFtsY, and 100 μM GTP doped with [γ-^{32}P]GTP. The cpFtsY concentration dependence of the observed GTPase rate constant (k_{obsd}) was fit to Equation 6,

$$k_{obsd} = k_{cat} \times \frac{[\text{cpFtsY}]}{K_m + [\text{cpFtsY}]} \quad \text{(Eq. 6)}$$

in which k_{cat} is the rate constant at saturating cpFtsY concentrations, and K_m is the concentration of cpFtsY at a half-maximal rate.

Basal GTPase activities of cpSRP54 and cpFtsY were measured under single turnover conditions, with trace [γ-^{32}P]GTP (<1 nM) and indicated concentrations of protein. The protein concentration dependence of observed rate constants was fit to Equation 7 as described previously (22, 26),

$$k_{obsd} = k_{max} \times \frac{[\text{protein}]}{K_{1/2} + [\text{protein}]} \quad \text{(Eq. 7)}$$

in which k_{max} is the maximal rate constant at saturating protein concentration, and $K_{½}$ is the protein concentration required to reach half the maximal rate.

Cross-linking—Complex formation between cpSRP54 and cpFtsY was carried out at 25 °C for 1–2 h in assay buffer (pH 7.0) using 10 μM cpSRP54, 10 μM cpFtsY, and 1 mM GppNHp. A 20-fold excess of a clickable cross-linker, NHS-activated 2,2′-(hex-5-ynylazanediyl) diacetic acid (32), was incubated with protein at 37 °C for 30 min. The reaction was quenched with 1 M Tris (pH 7.5) for 30 min. Cross-linked bands were excised from a 4–12% gradient gel after SDS-PAGE and digested with trypsin overnight at 37 °C (32). Extracted peptides were dissolved in 1% formic acid, desalted using a OMIX-C18 tip, and fractionated using SCX ion exchange resin with salt gradients (50–500 mM ammonium acetate) to enrich cross-linked peptides.

Mass Spectrometry and Data Analysis—NanoLC-MS/MS analyses were carried out on an LTQ Orbitrap (Thermo Fisher Scientific, Waltham, MA) with a nanospray interface coupled to an EASY-nLC pump (Proxeon, now Thermo Fisher Scientific). A 5-μl sample was loaded on a self-packed 5-μm Reprosil C_{18AQ} (Dr. Maisch GmbH, Ammerbuch-Entringen, Germany) column (75 μm × 150 mm). Mobile phase A was acetonitrile/formic acid/H_2O (2:0.2:98, v/v/v), and mobile phase B was acetonitrile/H_2O/formic acid (80:20:0.2, v/v/v). An 89-min gradient was used to separate the peptides. The gradient started at 0% B and increased linearly up to 33% within 80 min and was increased to 100% B in 1 min and held at 100% B for 8 min. The flow rate was 350 nl/min.

The LTQ Orbitrap was operated in data-dependent mode with full scan MS performed in the Orbitrap and a dependent MS/MS in the LTQ. The ESI spray voltage was 2.10 kV, and the capillary temperature was 200 °C. All spectra were acquired in positive mode in the range between *m/z* 300 and 2000 at a resolution of 60,000 at *m/z* 400. Collision-induced dissociation was performed in the ion trap with a 35% normalized collision energy at the default activation *Q* of 0.250 and activation time of 30 ms. Charge state screening and rejection were enabled, and only charge states of the precursor ion ≥ +2 were accepted. The 10 most intense peptide ions were isolated using the following parameters: dynamic exclusion setting, 1; repeated count, over

30 s; and exclusion duration, 90 s. XCalibur 2.0.7 (Thermo Scientific) was used as a control for both the EASY n-LC and the Orbitrap MS/MS.

Raw data were converted to MGF files using ReAdW4Mascot2. MGF files were searched using Protein Prospector Batch-Tag Web against cpSRP54 and cpFtsY. Digestion enzyme was specified as trypsin with up to three missed cleavages. The cross-linker was user defined with composition $C_{10}H_{11}O_2N_1$, reacting at Lys and the protein N terminus. MS1 tolerance was set at 10 ppm and MS2 tolerance was set at 0.5 Da. Variable modifications included oxidation of methionine and carbamidomethylation of cysteine.

Sequence Alignments—cpSRP54 and cpFtsY sequences from diverse organisms were obtained from NCBI BLAST searches and aligned using ClustalW provided by the NPS server (33). The phylogenetic tree was generated using PhyloT software and exported from iTOL (34, 35).

Structural Prediction—A structural model for the cpSRP54 M-domain was generated by the structural homology modeling program hosted by Swiss Model Workspace (36, 37), using the cpSRP54 M-domain sequence and the crystal structure of Ffh M-domain (Protein Data Bank code 2FFH). Electrostatic surface potential was generated using this homology model and PyMOL (The PyMOL Molecular Graphics System, Version 1.8 Schrödinger, LLC).

Author Contributions—S. S. conceived and coordinated the study and wrote the paper. S. C. designed, performed, and analyzed the experiments shown in Figs. 1–5, carried out the analyses in Fig. 6 and Table 1, and wrote the paper. S. C., C. H. S., S. H., and M. J. S. designed, performed, and analyzed the experiments shown in Fig. 2 and Table 1. All authors reviewed the results and approved the final version of the manuscript.

Acknowledgments—We thank Jesse Beauchamp for helpful discussions on the cross-linking and mass spectrometry experiments; members of the Proteome Exploration Laboratory for help with mass spectrometry experiments and analyses; the Guttman laboratory for help with phylogenic analysis, and members of the Shan laboratory for comments on the manuscript. The Proteome Exploration Laboratory was supported by the Beckman Institute and the Gordon and Betty Moore Foundation through Grant GBMF775.

References

1. Koch, H. G., Moser, M., and Müller, M. (2003) Signal recognition particle-dependent protein targeting, universal to all kingdoms of life. *Rev. Physiol. Biochem. Pharmacol.* **146,** 55–94
2. Walter, P., and Johnson, A. E. (1994) Signal sequence recognition and protein targeting to the endoplasmic reticulum membrane. *Annu. Rev. Cell Biol.* **10,** 87–119
3. Cross, B. C., Sinning, I., Luirink, J., and High, S. (2009) Delivering proteins for export from the cytosol. *Nat. Rev. Mol. Cell Biol.* **10,** 255–264
4. Keenan, R. J., Freymann, D. M., Stroud, R. M., and Walter, P. (2001) The signal recognition particle. *Annu. Rev. Biochem.* **70,** 755–775
5. Akopian, D., Shen, K., Zhang, X., and Shan, S. O. (2013) Signal recognition particle: an essential protein-targeting machine. *Annu. Rev. Biochem.* **82,** 693–721
6. Zopf, D., Bernstein, H. D., Johnson, A. E., and Walter, P. (1990) The methionine-rich domain of the 54 kd protein subunit of the signal recognition particle contains an RNA binding site and can be cross-linked to a signal sequence. *EMBO J.* **9,** 4511–4517
7. Zopf, D., Bernstein, H. D., and Walter, P. (1993) GTPase domain of the 54-kD subunit of the mammalian signal recognition particle is required for protein translocation but not for signal sequence binding. *J. Cell Biol.* **120,** 1113–1121
8. Halic, M., Blau, M., Becker, T., Mielke, T., Pool, M. R., Wild, K., Sinning, I., and Beckmann, R. (2006) Following the signal sequence from ribosomal tunnel exit to signal recognition particle. *Nature* **444,** 507–511
9. Bourne, H. R., Sanders, D. A., and McCormick, F. (1991) The GTPase superfamily: conserved structure and molecular mechanism. *Nature* **349,** 117–127
10. Connolly, T., Rapiejko, P. J., and Gilmore, R. (1991) Requirement of GTP hydrolysis for dissociation of the signal recognition particle from its receptor. *Science* **252,** 1171–1173
11. Shan, S. O., Stroud, R. M., and Walter, P. (2004) Mechanism of association and reciprocal activation of two GTPases. *PLoS Biol.* **2,** e320
12. Eichacker, L. A., and Henry, R. (2001) Function of a chloroplast SRP in thylakoid protein export. *Biochim. Biophys. Acta* **1541,** 120–134
13. Cline, K. (1986) Import of proteins into chloroplasts. Membrane integration of a thylakoid precursor protein reconstituted in chloroplast lysates. *J. Biol. Chem.* **261,** 14804–14810
14. Schuenemann, D., Gupta, S., Persello-Cartieaux, F., Klimyuk, V. I., Jones, J. D., Nussaume, L., and Hoffman, N. E. (1998) A novel signal recognition particle targets light-harvesting proteins to the thylakoid membranes. *Proc. Natl. Acad. Sci. U.S.A.* **95,** 10312–10316
15. DeLille, J., Peterson, E. C., Johnson, T., Moore, M., Kight, A., and Henry, R. (2000) A novel precursor recognition element facilitates posttranslational binding to the signal recognition particle in chloroplasts. *Proc. Natl. Acad. Sci. U.S.A.* **97,** 1926–1931
16. Zhang, L., and Aro, E. M. (2002) Synthesis, membrane insertion and assembly of the chloroplast-encoded D1 protein into photosystem II. *FEBS Lett.* **512,** 13–18
17. Tu, C. J., Schuenemann, D., and Hoffman, N. E. (1999) Chloroplast FtsY, chloroplast signal recognition particle, and GTP are required to reconstitute the soluble phase of light-harvesting chlorophyll protein transport into thylakoid membranes. *J. Biol. Chem.* **274,** 27219–27224
18. Franklin, A. E., and Hoffman, N. E. (1993) Characterization of a chloroplast homologue of the 54-kDa subunit of the signal recognition particle. *J. Biol. Chem.* **268,** 22175–22180
19. Li, X., Henry, R., Yuan, J., Cline, K., and Hoffman, N. E. (1995) A chloroplast homologue of the signal recognition particle subunit SRP54 is involved in the posttranslational integration of a protein into thylakoid membranes. *Proc. Natl. Acad. Sci. U.S.A.* **92,** 3789–3793
20. Träger, C., Rosenblad, M. A., Ziehe, D., Garcia-Petit, C., Schrader, L., Kock, K., Richter, C. V., Klinkert, B., Narberhaus, F., Herrmann, C., Hofmann, E., Aronsson, H., and Schünemann, D. (2012) Evolution from the prokaryotic to the higher plant chloroplast signal recognition particle: the signal recognition particle RNA is conserved in plastids of a wide range of photosynthetic organisms. *Plant Cell* **24,** 4819–4836
21. Rosenblad, M. A., Trager, C., and Schunemann, D. (2013) Structural diversity of signal recognition particle RNAs in plastids. *Plant Signal. Behav.* **8,** 10.4161/psb.26848
22. Peluso, P., Shan, S. O., Nock, S., Herschlag, D., and Walter, P. (2001) Role of SRP RNA in the GTPase cycles of Ffh and FtsY. *Biochemistry* **40,** 15224–15233
23. Zhang, X., Rashid, R., Wang, K., and Shan, S. O. (2010) Sequential checkpoints govern substrate selection during cotranslational protein targeting. *Science* **328,** 757–760
24. Shen, K., Arslan, S., Akopian, D., Ha, T., and Shan, S. O. (2012) Activated GTPase movement on an RNA scaffold drives co-translational protein targeting. *Nature* **492,** 271–275
25. Shen, K., Wang, Y., Hwang Fu, Y. H., Zhang, Q., Feigon, J., and Shan, S. O. (2013) Molecular mechanism of GTPase activation at the signal recognition particle (SRP) RNA distal end. *J. Biol. Chem.* **288,** 36385–36397
26. Jaru-Ampornpan, P., Chandrasekar, S., and Shan, S. O. (2007) Efficient interaction between two GTPases allows the chloroplast SRP pathway to bypass the requirement for an SRP RNA. *Mol. Biol. Cell* **18,** 2636–2645
27. Jaru-Ampornpan, P., Nguyen, T. X., and Shan, S. O. (2009) A distinct mechanism to achieve efficient signal recognition particle (SRP)-SRP re-

ceptor interaction by the chloroplast srp pathway. *Mol. Biol. Cell* **20,** 3965–3973
28. Chandrasekar, S., Chartron, J., Jaru-Ampornpan, P., and Shan, S. O. (2008) Structure of the chloroplast signal recognition particle (SRP) receptor: domain arrangement modulates SRP-receptor interaction. *J. Mol. Biol.* **375,** 425–436
29. Wild, K., Bange, G., Motiejunas, D., Kribelbauer, J., Hendricks, A., Segnitz, B., Wade, R. C., and Sinning, I. (2016) Structural basis for conserved regulation and adaptation of the signal recognition particle targeting complex. *J. Mol. Biol.* **428,** 2880–2897
30. Stengel, K. F., Holdermann, I., Wild, K., and Sinning, I. (2007) The structure of the chloroplast signal recognition particle (SRP) receptor reveals mechanistic details of SRP GTPase activation and a conserved membrane targeting site. *FEBS Lett.* **581,** 5671–5676
31. Nguyen, T. X., Chandrasekar, S., Neher, S., Walter, P., and Shan, S. O. (2011) Concerted complex assembly and GTPase activation in the chloroplast signal recognition particle. *Biochemistry* **50,** 7208–7217
32. Sohn, C. H., Agnew, H. D., Lee, J. E., Sweredoski, M. J., Graham, R. L., Smith, G. T., Hess, S., Czerwieniec, G., Loo, J. A., Heath, J. R., Deshaies, R. J., and Beauchamp, J. L. (2012) Designer reagents for mass spectrometry-based proteomics: clickable cross-linkers for elucidation of protein structures and interactions. *Anal. Chem.* **84,** 2662–2669
33. Combet, C., Blanchet, C., Geourjon, C., and Deléage, G. (2000) NPS@: network protein sequence analysis. *Trends Biochem. Sci.* **25,** 147–150
34. Letunic, I., and Bork, P. (2011) Interactive Tree Of Life v2: online annotation and display of phylogenetic trees made easy. *Nucleic Acids Res.* **39,** W475–W478
35. Letunic, I., Doerks, T., and Bork, P. (2012) SMART 7: recent updates to the protein domain annotation resource. *Nucleic Acids Res.* **40,** D302–D305
36. Arnold, K., Bordoli, L., Kopp, J., and Schwede, T. (2006) The SWISS-MODEL workspace: a web-based environment for protein structure homology modelling. *Bioinformatics* **22,** 195–201
37. Bordoli, L., Kiefer, F., Arnold, K., Benkert, P., Battey, J., and Schwede, T. (2009) Protein structure homology modeling using SWISS-MODEL workspace. *Nat. Protoc.* **4,** 1–13
38. Chu, F., Shan, S. O., Moustakas, D. T., Alber, F., Egea, P. F., Stroud, R. M., Walter, P., and Burlingame, A. L. (2004) Unraveling the interface of signal recognition particle and its receptor by using chemical cross-linking and tandem mass spectrometry. *Proc. Natl. Acad. Sci. U.S.A.* **101,** 16454–16459
39. Shen, K., and Shan, S. O. (2010) Transient tether between the SRP RNA and SRP receptor ensures efficient cargo delivery during cotranslational protein targeting. *Proc. Natl. Acad. Sci. U.S.A.* **107,** 7698–7703
40. Estrozi, L. F., Boehringer, D., Shan, S. O., Ban, N., and Schaffitzel, C. (2011) Cryo-EM structure of the *E. coli* translating ribosome in complex with SRP and its receptor. *Nat. Struct. Mol. Biol.* **18,** 88–90
41. Shan, S. O., and Walter, P. (2005) Molecular crosstalk between the nucleotide specificity determinant of the SRP GTPase and the SRP receptor. *Biochemistry* **44,** 6214–6222
42. Richter, C. V., Träger, C., and Schünemann, D. (2008) Evolutionary substitution of two amino acids in chloroplast SRP54 of higher plants cause its inability to bind SRP RNA. *FEBS Lett.* **582,** 3223–3229
43. Dünschede, B., Träger, C., Schröder, C. V., Ziehe, D., Walter, B., Funke, S., Hofmann, E., and Schünemann, D. (2015) Chloroplast SRP54 was recruited for posttranslational protein transport via complex formation with chloroplast SRP43 during land plant evolution. *J. Biol. Chem.* **290,** 13104–13114
44. Greber, B. J., Boehringer, D., Leibundgut, M., Bieri, P., Leitner, A., Schmitz, N., Aebersold, R., and Ban, N. (2014) The complete structure of the large subunit of the mammalian mitochondrial ribosome. *Nature* **515,** 283–286
45. Brown, A., Amunts, A., Bai, X. C., Sugimoto, Y., Edwards, P. C., Murshudov, G., Scheres, S. H., and Ramakrishnan, V. (2014) Structure of the large ribosomal subunit from human mitochondria. *Science* **346,** 718–722
46. Shen, K., Zhang, X., and Shan, S. O. (2011) Synergistic actions between the SRP RNA and translating ribosome allow efficient delivery of the correct cargos during cotranslational protein targeting. *RNA* **17,** 892–902
47. Egea, P. F., Shan, S. O., Napetschnig, J., Savage, D. F., Walter, P., and Stroud, R. M. (2004) Substrate twinning activates the signal recognition particle and its receptor. *Nature* **427,** 215–221

Co-evolution of Two GTPases Enables Efficient Protein Targeting in an RNA-less Chloroplast Signal Recognition Particle Pathway

Sowmya Chandrasekar, Michael J. Sweredoski, Chang Ho Sohn, Sonja Hess and Shu-ou Shan

J. Biol. Chem. 2017, 292:386-396.
doi: 10.1074/jbc.M116.752931 originally published online November 28, 2016